Structural Elucidation of Microporous and Mesoporous Catalysts and Molecular Sieves by High-Resolution Electron Microscopy

JOHN MEURIG THOMAS,*,† OSAMU TERASAKI,‡ PRATIBHA L. GAI,§ WUZONG ZHOU,|| AND JOSE GONZALEZ-CALBET⊥

Davy Faraday Research Laboratory, The Royal Institution of Great Britain, 21 Albemarle Street, London, U.K., Department of Materials Science, University of Cambridge, Cambridge CB2 1QY, U.K., Department of Physics and CREST (JST), Graduate School of Sciences, Tohoku University, Sendai 980-77, Japan, Central Research and Development Laboratories, DuPont, Experimental Station, Wilmington, Delaware 19880-0356, Department of Materials Science, University of Delaware, Newark, Delaware 19716, School of Chemistry, The University of St. Andrews, Fife KY16 9ST, Scotland, and Departmento de Quimica Inorganica, Facultdad de Quimicas, Universidad Compultense, 28040 Madrid, Spain

Received October 16, 2000

ABSTRACT

Twenty years ago, one of us embarked (Bursill, L. A.; Lodge, E. A.; Thomas, J. M. Zeolitic structures as revealed by high-resolution electron microscopy. *Nature* **1980**, *286*, 111−113) on the study of zeolites (renowned for their electron-beam sensitivity) by high-resolution transmission electron microscopy (HRTEM). In the ensuing years, high-resolution imaging aided by optical diffractometry has yielded details of the open framework structures of a number of new aluminosilicate and aluminophosphate molecular sieves and catalysts. The nature of intergrowth and recurrently twinned structures, as well as new types of structural imperfection in hitherto uncharacterized materials, has also been elucidated. With continued improvements in instrumental development, encompassing higher accelerating voltages, better objective lenses and vacua, computational advances, and the arrival of slow-scan CCD detectors, electron crystallographic methods and HRTEM imaging now enable the ab initio three-dimensional structures of micro- and mesoporous solids, with their occluded structure-directing organic species, to be determined. High-resolution scanning transmission electron microscopy using subnanometric probes provides supplementary structural and ultramicro analytical information and electron spectroscopic imaging (at the attogram level). In its high-angle annular dark-field mode, it is capable of locating and determining the composition of individual nanoparticle catalysts (consisting of just a few atoms) supported on porous hosts.

1. Introduction

Ever since a zeolite (idealized formula $M_{x/m}[Al_xSi_{1-x}O_2]\cdot nH_2O$, where M is a cation of valence m) with no natural counterpart was first synthesized in the late 1940s, microporous solids have moved inexorably, and of late with remarkable rapidity, to occupy places of high prominence in the landscape of solid-state and materials science, heterogeneous catalysis, and clean technology. First, there came synthetic zeolite type A; then, in the 1960s, crystalline faujasitic zeolites, and zeolite Y in its La^{3+} exchanged form in particular, displaced amorphous silica−alumina as strongly acidic cracking catalysts for the conversion of oil to useful products. Soon there followed the pentasil family of molecular sieve catalysts (i.e., synthetic aluminosilicates typified by ZSM-5 and ZSM-11 now designated MFI and MEL, respectively) and their corresponding siliceous adsorbents (i.e., silicalite-1 and silicalite-2) which, functioning in a shape-selective manner, were remarkably effective in a range of alkylations, isomerizations, and dehydrative syntheses (such as the production of olefins and gasoline from methanol), as well as in a variety of delicate molecular separations.

In the early 1980s there emerged[2] a large, new family of microporous aluminophosphates (ALPOs). Not only were there many ALPOs (or MAPOs, framework-substituted metal aluminophosphates where M could be Mg, Mn, Zn, Co, Fe, etc.) that exhibited framework structures that were the same as those of either natural or synthetic (aluminosilicate) zeolites, but there were also novel open-framework structures with no counterparts in the zeolitic world. Thus, the framework of AlPO-17 is the same as that of erionite, and the framework of AlPO-5 (AFI) is the same

* To whom correspondence should be addressed.
† The Royal Institution of Great Britain and University of Cambridge.
‡ Tohoku University.
§ DuPont and University of Delaware.
|| The University of St. Andrews.
⊥ Universidad Compultense.

John Meurig Thomas's interest in the electron microscope began at the University College of North Wales, Bangor, where he started his lecturing career. His interests have roamed widely within the realm of solid-state and materials chemistry, especially in the design, synthesis, and in situ characterization of new molecular sieve catalysts. He was Director of the Royal Institution of Great Britain from 1986 to 1991 and gave the annual Christmas lectures (on crystals), which were televised nationally by the BBC in 1987. He was knighted in 1991 for his services to chemistry and the popularization of science.

Osamu Terasaki joined the Physics Department of Tohoku University, Sendai, as a faculty member in 1967, immediately after receiving his M.Sc. from Tohoku University. He studied structures of the Ti−O system, incommensurate Au-based alloys, and electron dynamic scattering phenomena. In 1982, he started studying fine structures of zeolites with Sir John Meurig Thomas at the University of Cambridge as a Guest Research Fellow of the Royal Society. He was also a guest professor at Lund University, Sweden, in 1987.

Pratibha L. Gai completed her Ph.D. in physics at the Cavendish Laboratory, University of Cambridge, in 1974, after receiving her initial M.Sc. degree from the Indian Institute of Technology, Mumbai. She was Group Leader of Surface Sciences at the Department of Materials, University of Oxford (1976−1988), and a Fellow of Wolfson College. Since 1988, she has held joint appointments at the DuPont Central Research and Development Analytical Sciences, where she heads the microstructural competency section, and at the University of Delaware, where she is a joint/adjunct Professor of Materials Science. She is a Fellow of the Institute of Physics and Fellow of the Royal Microscopical Society.

Wuzong Zhou received his B.S. degree at Fudan University, Shanghai, and completed his Ph.D. on electron microscopy in Sir John Meurig Thomas's group at the University of Cambridge, U.K., in 1988. He is currently Reader in chemistry at the University of St. Andrews, Scotland.

Jose M. Gonzalez-Calbet received his initial degree at Universidad Compultense in Madrid, Spain. He joined the Physical Chemistry Department at Cambridge University (UK) (1980−1982), where he broadened his interest in the microstructural characterization of zeolites in joint work with John Meurig Thomas. He has been full Professor of Inorganic Chemistry and head of the Inorganic Chemistry Department at Universidad Compultense since 1994.

10.1021/ar970352j CCC: $20.00
Published on Web 05/05/2001

as that of SSZ-24, the only difference being that corner-sharing AlO_4 and PO_4 tetrahedra alternate in the former in place of AlO_4 and SiO_4 in erionite and faujasite (which is the framework structure of zeolites X and Y). But AlPO-36,[3] DAF-1[4] (also known as DFO), and many other so-called zeotypes have no counterparts in aluminosilicate chemistry.

Also in the early 1980s, Italian workers discovered that Ti^{IV} ions, isomorphously substituted for Si^{IV} in open frameworks, yielded TS-1 and TS-2 (which are structurally identical, except for the framework substitution of Ti^{IV} ions to MFI and MEL, respectively) that are powerful catalysts in a wide range of selective oxidations. Later, another novel open-structure titanosilicate[5] ETS-10 was also found to be catalytically active. Since 1998, it has emerged that certain framework-substituted ALPOs are exceptionally good catalysts for the regioselective functionalization of alkanes in air or oxygen.[6]

Mesoporous silicas, notably those designated FSM[7] (produced from the layered silicate mineral kanemite ($NaHSiO_3 \cdot 3H_2O$)) and MCM-41[8] (produced from a range of surfactant or liquid crystal templates), have greatly expanded the opportunities presented to pure and applied scientists in that pore diameters from 15 to over 300 Å may be controllably prepared as catalyst supports, adsorbents, and membranes. Particularly useful is that it is much simpler than originally thought for heteroatoms (e.g., transition-metal redox ions) to be incorporated, either during or after synthesis, into the frameworks of both micro- and mesoporous silicas. Novel organic–inorganic hybrid mesoporous materials have also recently been synthesized in which organic and inorganic moieties are distributed uniformly at the atomic level in their frameworks. Moreover, it is relatively easy, aided[9] by the adroit choice of organic template present in the nutrient mixture from which the molecular sieves crystallize, to produce a wide range of microporous gallophosphates, cobalt aluminophosphates, zincophosphates borates, oxides, chalcogenides,[10] and other ordered microporous solids.[3] With the high-area and thermally stable mesoporous supports, new opportunities exist not only for heterogenizing homogeneous catalysts,[11,12] but also for assembling biomimetic or ship-in-a-bottle (tea bag[13]) catalysts as well as spatially constrained chiral catalysts for enantioselective conversions.[14] There is also much scope for harnessing quantum confinement effects and for probing low-dimensional electronic and magnetic properties associated with arrays of metal clusters and metal nanowires tightly packed in the channels of mesopore hosts.[15]

Over half of all the elements of the Periodic Table may be incorporated during or after synthesis into the framework structures of micro- and mesoporous solids. If we include incorporation into extraframework sites, the fraction rises to beyond three-quarters.

Notwithstanding the prodigality of preparative successes witnessed in this area of chemical research, acute difficulties have been encountered in elucidating the structures of the resulting solids. The reasons for this state of affairs are several:

(i) Most zeotypic materials are microcrystalline (particle dimension 1 μm or less) and are frequently too small to be amenable to structure determination by single-crystal X-ray methods, even allowing for recent advances[16] in (micro) single-crystal X-ray analysis using synchrotron sources, or for recent dramatic successes in structural elucidation using Monte Carlo (direct space) genetic alogorithms.[17]

(ii) Many microporous zeotypes[18,19] and some mesoporous solids[20] exhibit a marked tendency to form intergrowths with closely similar structures. These intergrowths may be isolated, recurrent, or nonrecurrent or may coexist with the parent structure as discrete slabs, thus complicating, often to the intractable limit,[21] the resulting X-ray diffraction patterns.

(iii) Conventional X-ray diffraction methods are, in general, ill-suited to probe the location and internal structure of nanoparticle catalysts (e.g., mono- or bimetallic).[22] Moreover, extraframework guest species have a tendency to be distributed in a spatially nonuniform fashion (as is the case with selenium in mordenite[23]) inside a zeotypic host, and low concentrations of framework-substituted ions (e.g., Co^{III} in CoAlPO alkane oxidation catalysts[6]) do not adopt superlattice structures, thereby making X-ray diffraction analysis almost impossible. Even when superlattices form, it is still very difficult to observe weak superlattice reflections by powder X-ray diffraction methods.

(iv) It is extremely difficult to determine at atomic resolution the three-dimensional structure of mesoporous solids by X-ray diffraction methods. Mesoporous materials exhibit order on the mesoscale but disorder on the atomic scale; moreover, mesoscale order is extremely sensitive to synthesis conditions. But with high-resolution transmission electron microscopy from ultrathin regions coupled with digital Fourier analysis, their structures may be solved (see the case of MCM-48 below) from the measured amplitudes and phases.

2. The Advantages of High-Resolution Transmission Electron Microscopy (HRTEM)

It had become apparent[24,25] in the early 1970s that HRTEM was a powerful technique for the elucidation, in real space, of the ultrastructural features of many silicates and other minerals. Whereas X-ray-based techniques had yielded ambiguous (at best) information concerning the spatial character of polytypic intergrowths in chain silicates (of the pyroxenoid family, general formula $ASiO_3$ with A = Ca^{2+}, Mg^{2+}, Fe^{2+}, and Mn^{2+}, such as wollastonite, rhodonite, and pyroxmangite), HRTEM yielded precise and unambiguous information.[26] Likewise, triple-chain defects and other unusual structural features intergrown within regular double-chain silicates in amphiboles such as crocidolite and nephrite jade[27] could be directly imaged with HRTEM, and the correlation of structure type with composition within the serpentine minerals such as antigorite[28] was incontrovertibly established. Nonrandom

disorder in the rather exotic sheet silicates chloritoid and stilpnomelane[29] could also be directly probed by HRTEM and so also, for the first time, could the "staging" of guest layers in graphite intercalates, thereby leading to an atomistic mechanism for their interconversion.[30]

All the minerals cited above were sufficiently stable to withstand the irradiation from the intense electron beam of the high-resolution microscope, so they readily yielded their ultrastructural features (both perfect and imperfect) in HRTEM images with point-to-point resolutions of ca. 3−4 Å. Many more minerals, zeolites among them, awaited study via this powerful, new, direct (real-space) tool; however, initial experience showed that the majority of them degraded catastrophically during electron microscopic imaging.

With the arrival in the late 1970s of a new generation of commercial and custom-built electron microscopes, the situation improved greatly. The accelerating voltage of these instruments was 200 keV or higher, so the beam damage of sensitive specimens by ionization processes was greatly reduced. Moreover, there were improved vacua in these microscopes, thereby further diminishing beam damage. In addition, the coefficients of spherical aberration of the objective lenses were reduced, and the high-voltage stability (hence degree of monochromaticity) was greatly improved. All this meant that structures of, and imperfections in, a wide range of zeolites that were hitherto beyond reach could now be systematically explored.[18,31]

Recently, further advances have become possible owing to the development of charge-coupled devices (CCDs).[32] Since CCDs are more than 100 times as sensitive to electrons than photographic detectors, the problem of electron-beam sensitivity of specimens has been greatly diminished. Just as in X-ray crystallography, direct methods of structure determination by electron crystallography may be used, for example, to solve the structure of SSZ-48 (see below). One of us (J.M.G.-C.) and his co-workers were the first[33] to employ electron-diffraction intensity data for the ab initio determination of the structure of a new zeolite (MCM-22). (In ref 33, sensitive microdensitometry, using the classical Klug method[34] of three-dimensional image reconstruction, rather than CCDs was used to record diffraction intensities.)

3. Summary of the Basics of High-Resolution Electron Microscopy

It is instructive to summarize the three principal ways in which HRTEM has elucidated the structures of micro- and mesoporous solids. An image produced by HRTEM corresponds to a map of projected electrostatic potential for electrons along the direction of incidence of the beam (Figure 1a). Since atomic scattering amplitudes for electrons are approximately 10^4-10^5 times as large as they are for X-rays and neutrons, it follows that, with electrons as probes, structural information may be retrieved from single crystals of almost miniscule dimension. To illustrate

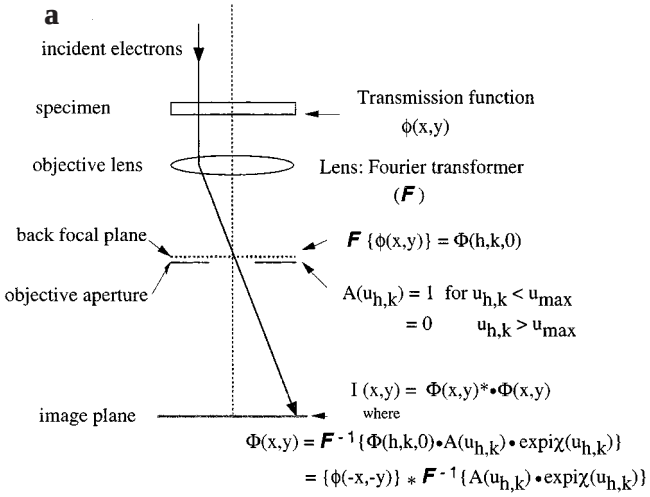

FIGURE 1. (a) The objective lens of a microscope serves as a Fourier transformer. The diffraction pattern formed at the back focal plane is further Fourier transformed to yield the image. There are phase changes in the electron waves for (*h*,*k*) reflections (*h* and *k* being indices in reciprocal space) as a function of wave vectors *u*(*h*,*k*). The phase contrast imaging performance of an HREM is governed by the contrast transfer function $\chi/u(h,k)$, which contains the spherical aberration coefficient of the lens and the extent of its defocus. $A(u(h,k))$ is an objective lens transfer function: the intensity $I(x,y)$ at the image plane is proportional to the projected electrostatic potential density in the "weak-phase" approximation. $\Phi(x,y)$ yields the structure in real space (the asterisk signifies convolution). (b) HRTEM image of germanium silicalite ($GeSiO_4$) in which there are channels of aperture diameter 0.55 nm running along [010] direction. The inset shows five- and six-membered smaller apertures that are circumjacent to larger (0.55 nm) channels.

this point, recall that even with the best attainable X-ray performance (with synchrotron sources), crystal dimensions of ca. $2 \times 2 \times 2$ $(\mu m)^3$ are required (i.e., some 10^9 or more unit cells for a typical micro- or mesoporous catalyst). Because of the strong interaction of electrons with atoms, only some 10^4 unit cells of the specimen signifying masses of sample as little as 10^{-18} g are needed to yield meaningful HRTEM image and diffraction pattern.

There are both fundamental and practical difficulties that demand great caution in the interpretation of such images. The strong interaction between electrons and atoms leads to multiple scatterings (i.e., dynamical phenomena), which are quite complex, though computable. In addition, electron lenses always contribute some degree of spherical aberration, and image information is also

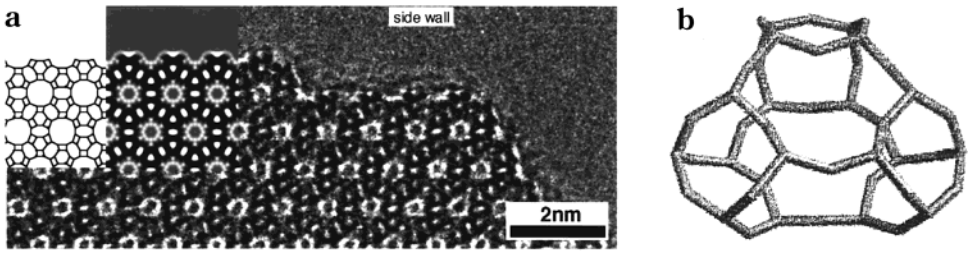

FIGURE 2. (a) HRTEM of L-type zeolite (LTL) along [001]. Schematic of the LTL structure and a computed image with a perfect match to HREM are inset (top left). Cancrinite cages (b) are clearly visible. (b) Schematic of a cancrinite cage (a major structural component of LTL).

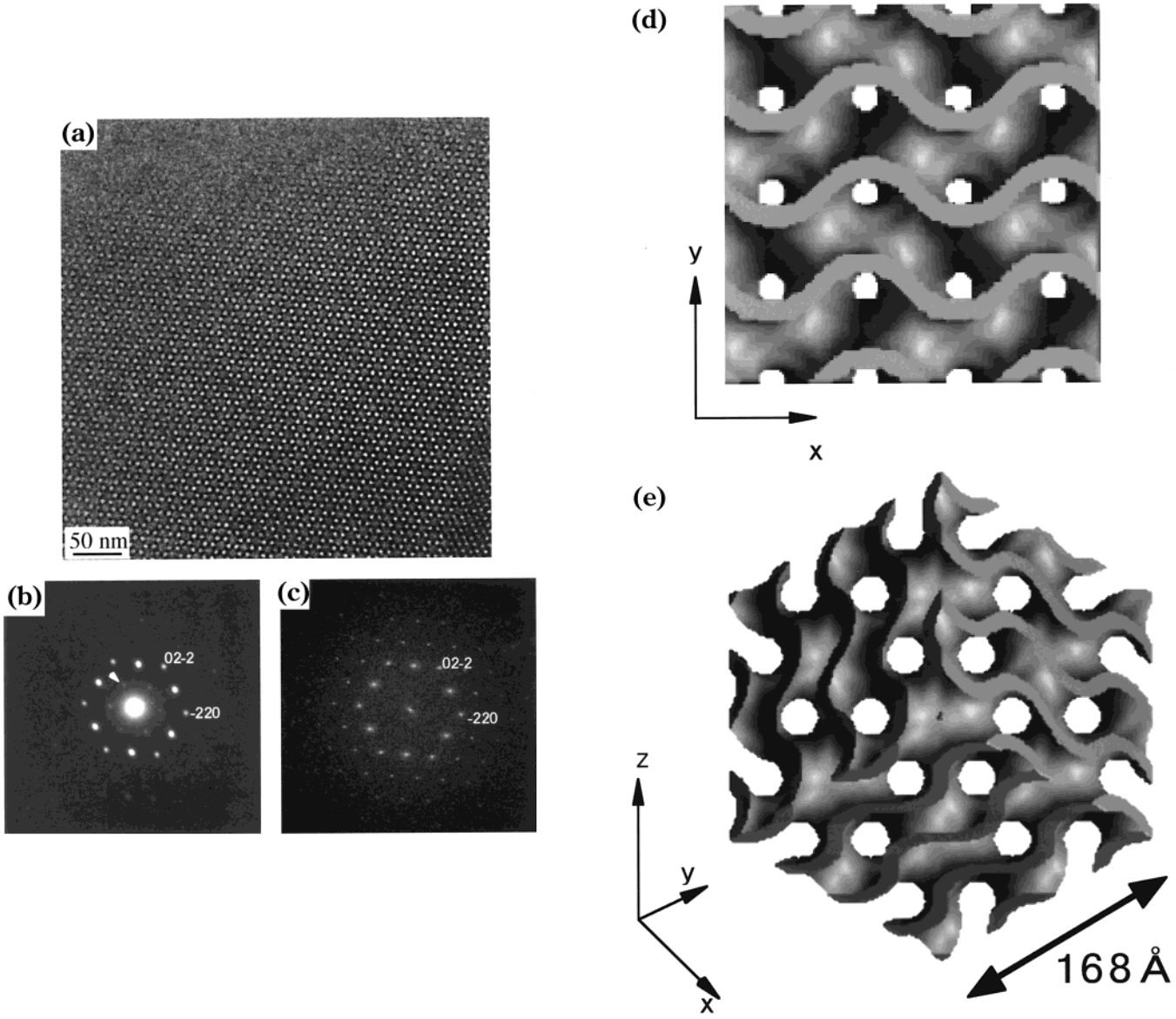

FIGURE 3. (a) HRTEM of MCM-48 along [111] with (b) electron diffraction (c) Fourier diffractogram of (a). (d,e) Structure of MCM-48 (d) along [100]; (e) is a 3D representation along [111].

limited by the chromatic aberration created by energy losses in the sample. It is now possible, also by computation, to make allowances for, and even to eliminate, the corruption of the image by spherical aberration, and by chromatic aberration with computation or energy-filtering. In practice, as explained elsewhere,[35] a convenient operational procedure in HRTEM is to record a series of images at a series of settings of lens defocus and as a function of sample thickness. By comparing an observed image with that computed through the well-proven multislice procedure[35] (for the conditions that apply in the imaging), a trustworthy result is obtained, as illustrated in Figure 2, for the near-surface structure of zeolite L.

Here, HRTEM shows that the structure of this zeolite remains unchanged right from the bulk to the outermost layer; there is none of the major changes that are often

seen in low-energy electron-diffraction studies of other solid oxides, such as chromia and alumina. The simulated images of the surface of zeolite type L—terminating with cancrinite cages—match very closely the actual HRTEM image. There is little evidence of contraction perpendicular to the surface.

A second method of retrieving structures from electron microscopy is the one pioneered by Klug[34] for determining the structures of viruses and other materials in molecular biology. This entails using the amplitudes from the intensities of the electron-diffraction spots and the extraction of the phases of the corresponding reflections from the high-resolution image. As is well known, phases are more important for solving the structure, while amplitudes are more important for refining it. As long as the phases are correct, errors in the amplitudes do not materially change the atomic positions. This procedure has not been applied routinely to inorganic structures (with a few notable exceptions) on complex oxides and chalcogenides[36] and on zeolites.[33] It has the great advantage of yielding a structure from about 10^4 unit cells.

With the availability of slow-scan CCD cameras and the recent digital revolution, it is routinely possible to treat the digital data of electron-diffraction (ED) patterns and HRTEM images recorded under low-dose conditions in a quantitatively rigorous manner.[37] Provided the precise experimental conditions (crystal thickness, degree of electron-beam tilt to the crystallographic axes, and extent of defocus) are known, one may solve the crystal structure using the theory of electron dynamic scattering. Even a quite low-resolution HRTEM image suffices for the phase recovery of the reflections. Figure 3 shows three-dimensional images of the $2 \times 2 \times 2$ unit cells of the mesoporous silica structure known as MCM-48. Crystals of MCM-48 are well-ordered over a large area, but the walls are amorphous and follow a so-called gyroid surface (a minimal surface).[37]

It is to be noted that the pore volume of MCM-48 is 0.84 $cm^3\ g^{-1}$ and that the wall density is 2.29 $g\ cm^{-3}$. The pore-to-volume ratio of this cubic mesoporous silica is 0.65.

4. High-Resolution Scanning Transmission Electron Microscopy (HRSTEM)

Images with this technique (see Figure 4) are formed by scanning a finely focused probe (ca. 0.8 nm) over a thin specimen. HRSTEM images have slightly diminished resolutions compared with analagous HRTEM ones because of the finite source size and the reduced detection efficiency imposed by the geometry of the collection. However, an HRSTEM image has at least two important advantages: First, it has ultrahigh-resolution microanalytical capabilities of X-ray (and visible light) emission and Auger and electron-energy loss spectroscopy, and second, all these signals may be collected simultaneously, together with backscattered electrons. Since HRSTEM readily yields high-angle annular dark-field (HAADF) images, as well as both bright-field (BF) images, formed

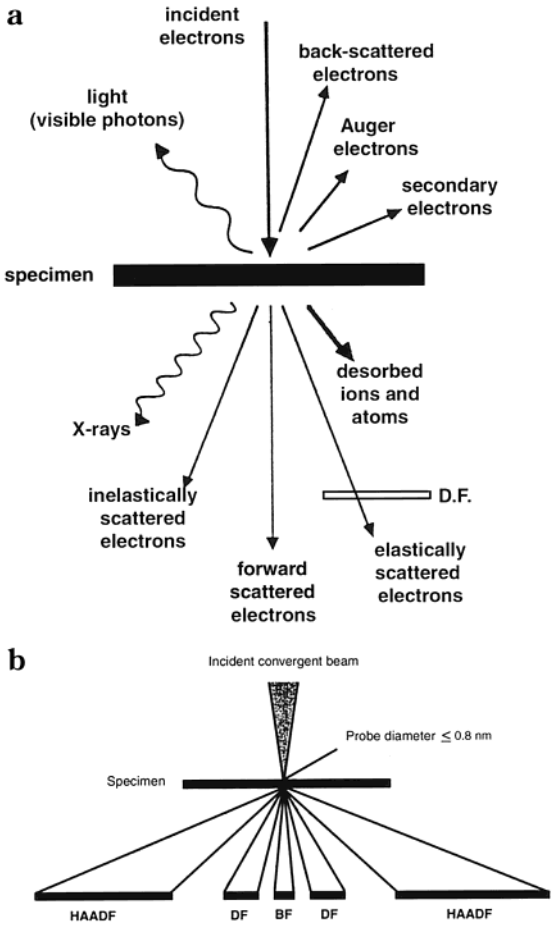

FIGURE 4. (a) Schematic of the information from HRSTEM. DF stands for dark field. (b) High-angle annular dark-field (HAADF) microscopy, which highlights heavy atoms on a light-atom support (see text and Figure 10 below).

from the transmitted electrons, and ordinary dark-field (DF) images, formed from Bragg scattered beams, there are extra benefits to be gained in locating nanoparticles composed of as little as two- or three-atom clusters.[22,38]

An important aspect of HRSTEM is *Z-contrast imaging* (or *atomic number imaging*), which exploits the fact that high-angle scattering intensity of electrons from thin specimens follows the Z^2 dependence of Rutherford's law, where Z is the atomic number. Thus one Pt atom scatters as strongly as about 100 oxygen atoms or 32 silicon atoms. The technique is tailor-made for detecting clusters of catalytically active metals or bimetals such as Pt, Pd, or Ru, or clusters thereof, on light supports such as zeolites, MAPOs, or mesoporous silica and alumina.[39a]

High-Precision Composition Analysis in the Electron Microscope. Composition analysis in the electron microscope by the various processes of inelastic scattering of electrons during the beam—sample interactions (see Figure 4) is particularly effective in studies of micro- and mesoporous catalysts and molecular sieves. Chemical analyses using electron probe sizes of a few nanometers or less are now possible in modern HRTEM/STEM, and they yield chemical composition at high spatial resolution, including stoichiometric and valence variations from areas of the order of 10 nm or less. Energy-dispersive X-ray

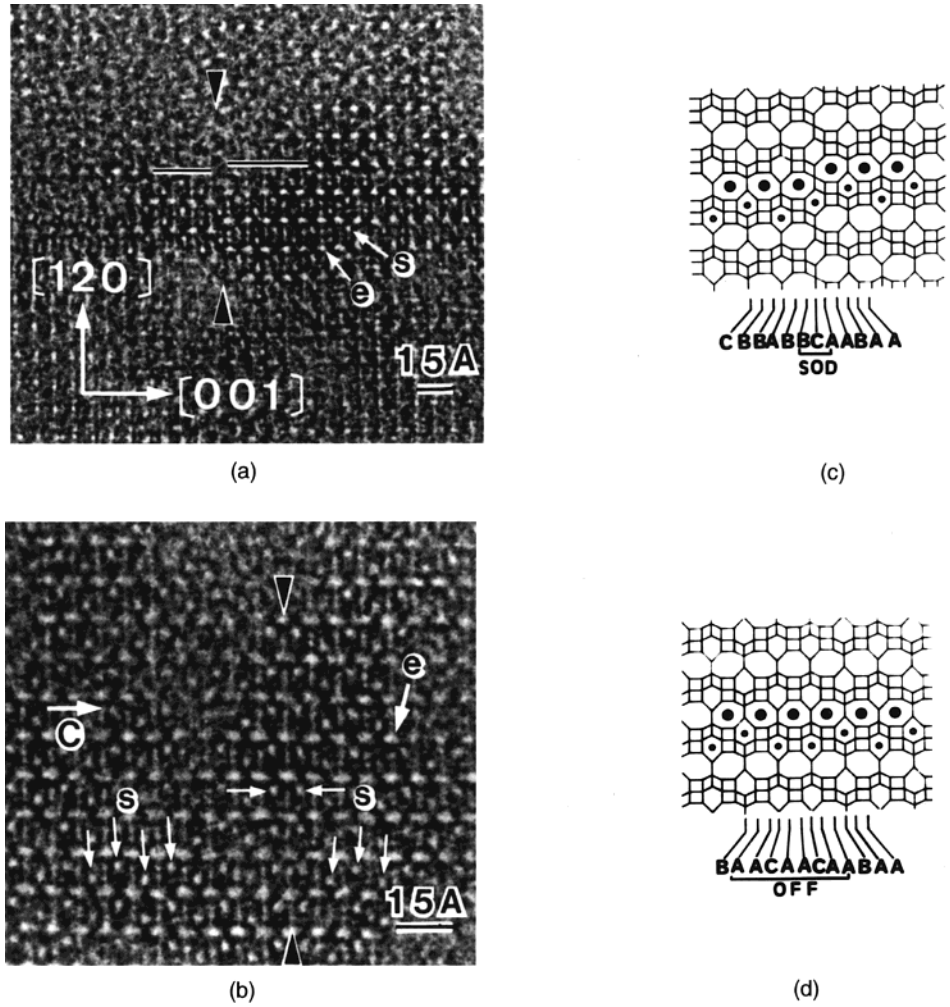

FIGURE 5. HRTEM of stacking defects in (a) a sodalite (SOD) and (b) offretite (OFF) defect in erionite (ERI), with schematics in (c) and (d). (The labels "e" and "s" refer to "eight-" and "six-"membered rings, denoted also by large and small dots, respectively, in the ERI structure.)

spectroscopy (EDX), where X-ray intensities are measured as a function of the X-ray energy, is the most convenient to use. Electron-induced energy-loss spectroscopy (EELS) is another method for chemical analysis, especially of light elements, the ratios of which may be determined to about ±5%.[39b] The development of parallel detectors in EELS (PEELS) enables fast acquisition rates and digital storage facilities. In addition to effecting compositional analysis, at high spatial resolution, it is often advantageous to probe the chemical homogeneity of a typical area or of entire crystals in a sample by analyzing variations in X-ray elemental mapping. Quantification of the X-ray intensities for chemical composition can provide relative amounts of the elements in the X-ray maps. In modern HRTEM/STEM instruments, X-ray elemental mapping is carried out digitally.

5. Case Histories

We now proceed to illustrate the power of HRTEM and HRSTEM in the elucidation of a variety of problems central to the theme of this Account.

(i) Coherent Intergrowths. Zeolites that belong to the family of ABC-6 zeolites may be regarded as having been assembled architecturally from individual sheets (thickness 2.6 Å) consisting of macroanions of corner-sharing SiO_4^{4-} and AlO_4^{5-} tetrahedra (Si:Al ranging from 1 to 4), there being occluded, charge-compensating cations, typically Na^+, Ca^{2+}, and K^+, and water. Cancrinite, in which the stacking sequence of the sheets may be symbolized as AB, has a 5.1 Å repeat along the direction of stacking; sodalite has ABC stacking, and erionite has AABAAC stacking. It had long been suspected on the basis of chemical and diffusive behavior that naturally occurring and synthetic analogues of this class of zeolite could, depending upon their genesis, form intergrowths at the unit-cell level, and the presence of such features would profoundly affect the catalytic and adsorptive performance of the parent zeolite. HRTEM proved the ideal technique[31] for directly attacking this problem. Figure 5 illustrates how real-space imaging, by readily distinguishing the size of the eight-ring (8R) and six-ring (6R) apertures, yields an unambiguous picture of the localized intergrowths that occur in erionite, a petrochemically important catalyst.

Such isolated or recurrent intergrowths had been identified earlier in ZSM-5 catalysts and in faujasite (FAU) and in those of its hexagonal analogue called EMT (Figure

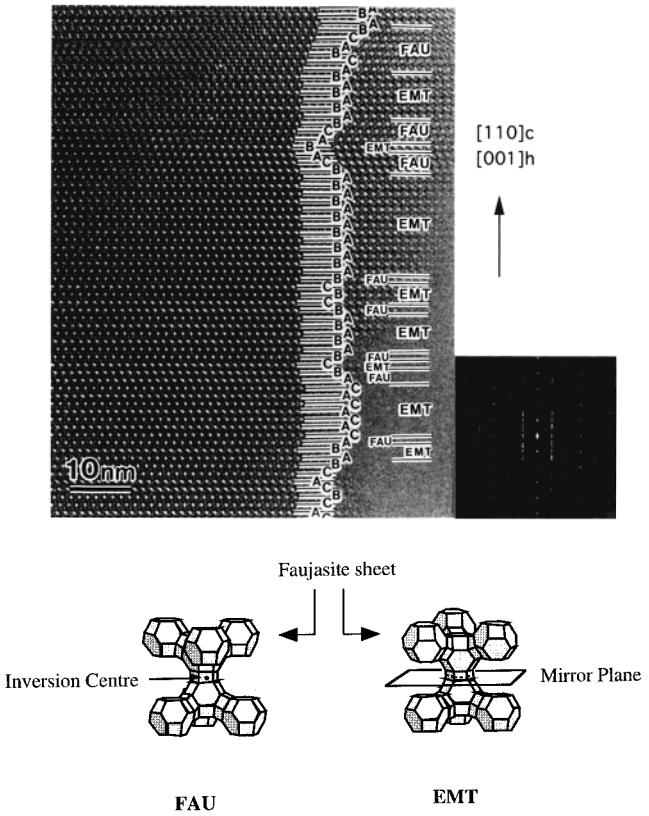

FIGURE 6. HRTEM of FAU/EMT intergrowths along [110]. The stackings ABC... and AB... correspond to the FAU and EMT structures, respectively.

6).[18] It is now clear, thanks to HRTEM, that the confusion that had arisen in the open and patent literature concerning the nature of rival catalysts (designated ZSM-3, ZSM-20, ECR-4, ECR-30, CSZ-1, and CSZ-3) is all intelligible[19] in terms of the precise nature of FAU and EMT intergrowths.

HRTEM imaging also unambiguously showed[40] that the structure of the synthetic zeolitic catalyst ECR-1 is an intimate twin of the natural zeolites mordenite and mazzite and that the synthetic zeolitic catalyst ZSM-23 (MTT) is a recurrently twinned[41] version of the synthetic zeolite theta-1 (TON), the original structure of which was determined in part by HRTEM studies[42] (Figure 7). HRTEM images of the L-type zeolite revealed[18,43] the existence of several types of coincidence boundaries, one unusual variant, based on a mesh of $\sqrt{13} \times \sqrt{13}$ times the hexagonal *a* dimension, being responsible for a greatly diminished diffusivity of reactant molecule to, or products from, active sites that are predominantly located (as with most zeolitic catalysts) on the inner surfaces of the crystal.

(ii) Solving the Atomic Structures of Microporous Catalysts. Here we illustrate two distinct approaches. For the framework-substituted aluminophosphate catalyst MAPO-36,[44a] a combined approach entailing computation and HRTEM imaging was used; for the high-silica large-pore SSZ-48[44b] material, electron-diffraction data were used as outlined earlier.

(a) MAPO-36 Microporous Catalysts. These materials, which are good aerial selective oxidation catalysts for hydrocarbons[6] and are beam-sensitive, yielded HRTEM

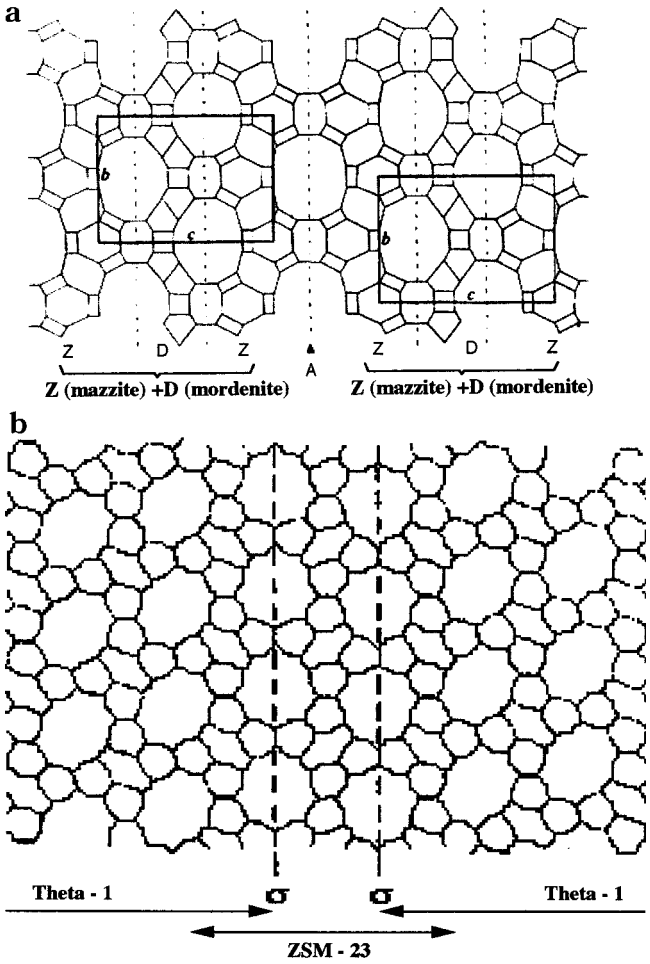

FIGURE 7. (a) HRTEM reveals the zeolite ECR-1 to be a sub-unit-cell intergrowth (recurrent) of mordenite and mazzite layers. (b) Schematic of ZSM-23 structure, revealed by HRTEM to be a recurrently twinned version of the zeolite theta-1 (TON).

images down high-symmetry directions that unmistakably revealed (Figure 8a) 12-ring channel systems similar to those in zeolite L (and in ALPO-5), the structure of which was readily solved by X-ray diffraction.[45] This is also in line with the results of gas adsorption studies. The crystal symmetry and the approximate values of the unit dimensions were all derived from the electron-diffraction pattern. These data yielded a plausible model for a structure that was then refined by the distance least-squared (DLS) technique,[46] working on the assumption of maximum symmetry *Cmcm* and disordered Al and P in the tetrahedral (T) sites. The resulting simulated X-ray diffraction (XRD) closely resembled the experimental pattern collected at high temperature but was not quite in line with that at low temperature. Lattice energy minimization calculations were then carried out[47] in which no symmetry constraints were applied and all atomic positions and all parameters were allowed to vary. The T sites were replaced by Si in a first simulation, and in the idealized composition $AlPO_4$, the T sites were replaced by ordered Al and P with appropriate partial charge potentials.[47] Proceeding along these lines, very good agreement was obtained between the simulated and experimental XRD patterns at both high

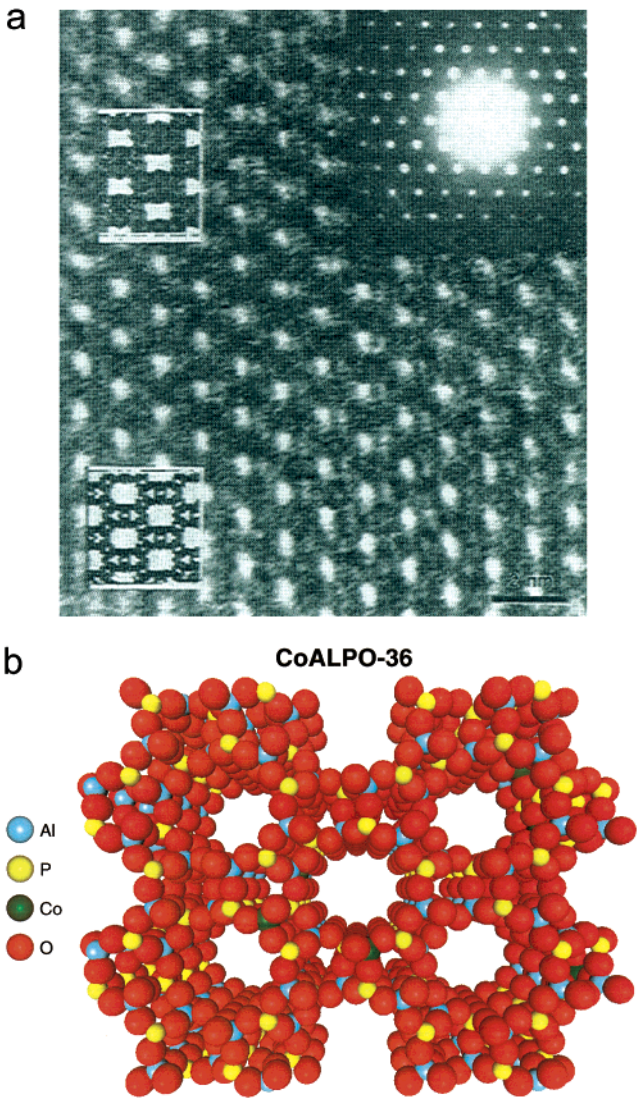

FIGURE 8. (a) HRTEM of CoAlPO-36 showing well-defined large apertures, and with the computed image inset, revealing the outline of 12-membered rings (top and bottom are with and without taking beam damage into account). (b) Combining data from (a) with other data, including atomistic calculations, an atomic-scale structure of the AlPO-36 framework with random distribution of Co^{II} ions is obtained.

and low temperature, and the energy-minimized atomic coordinates of the idealized $AlPO_4$ end-member of the CoAlPO-36 structure were derived (Figure 8b).

(b) The High-Silica Microporous Solid SSZ-48. Electron-diffraction intensity data were collected using a 400 keV microscope equipped with a slow-scan CCD detector. Integrated intensities for 600 reflections (326 unique ones) were extracted from 11 zone axes, and the diffraction data were collected to a resolution of 0.99 Å ($-8 < h < 8$, $-4 < k < 4$, $-10 < l < 13$) and merged by normalizing the diffraction data between zones containing common reflections. The indexation of these reflections revealed a monoclinic crystal having unit-cell dimensions $a = 11.19$ Å, $b = 4.99$ Å, and $c = 13.65$ Å, with $\beta = 100.7°$ ($V = 748.6$ Å^3). Systematic absences indicated a spare group $P2_1$. Reflections with normalized structure factors between

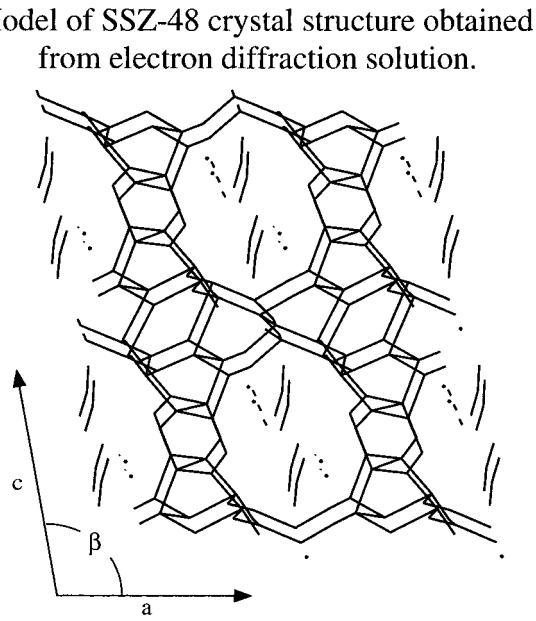

FIGURE 9. Structural model of the SSZ-48 crystal structure with projected positions of the organic template within the pores.

0.65 and 10.0 were used in the direct methods structure solution. The phases obtained from the direct methods structure solution were used to generate a 3D potential map that readily revealed the seven tetrahedrally coordinated silicon atoms in the asymmetric unit and five of the 14 oxygen atoms. The structure obtained in this way is shown in Figure 9. The remaining oxygen atoms in the framework were located using the DLS technique; the organic template (*N*,*N*-diethyl-decahydroquinolinium cation) was adjusted by energy minimization within the micropores of the refined framework. (The resulting structure was also confirmed by HRTEM direct imaging and by Rietveld refinements of the synchrotron powder-diffraction data.)

(iii) Nanoparticle Composition and Distribution in Bifunctional Catalysts. HRTEM, under optimal conditions, is capable of locating and identifying metal clusters in micro- or mesoporous supports when their diameters are not less than 10−15 Å. Tomography is also a possible method to locate the positions of clusters inside a zeolite. By taking HRTEM images from successive, ultrathin sections, it was confirmed that Pt clusters preferentially occupy the (111) twin planes of faujasitic zeolites.[48]

For reasons given earlier, HRSTEM surpasses HRTEM in identifying even smaller size clusters (consisting of as little as two or three atoms), as illustrated in bimetallic PdRu catalysts.[22] It had been shown by X-ray absorption spectroscopy[49] that thermolysis of the silica (MCM-41)-supported $(Pd_6Ru_6(CO)_{24})^{2-}$ anions yield discrete clusters of Pd_6Ru_6. Using HRSTEM (see Figure 4), both bright-field (BF) and HAADF images (Figure 10) of the bimetallic nanocluster are obtained, and the precise elemental distribution, acquired by collecting the emitted characteristic X-rays, is determined. From the exact correspondence of the Pd (X-ray) and Ru (X-ray) images, we conclude that the Pd_6Ru_6 nanoclusters remain intact in

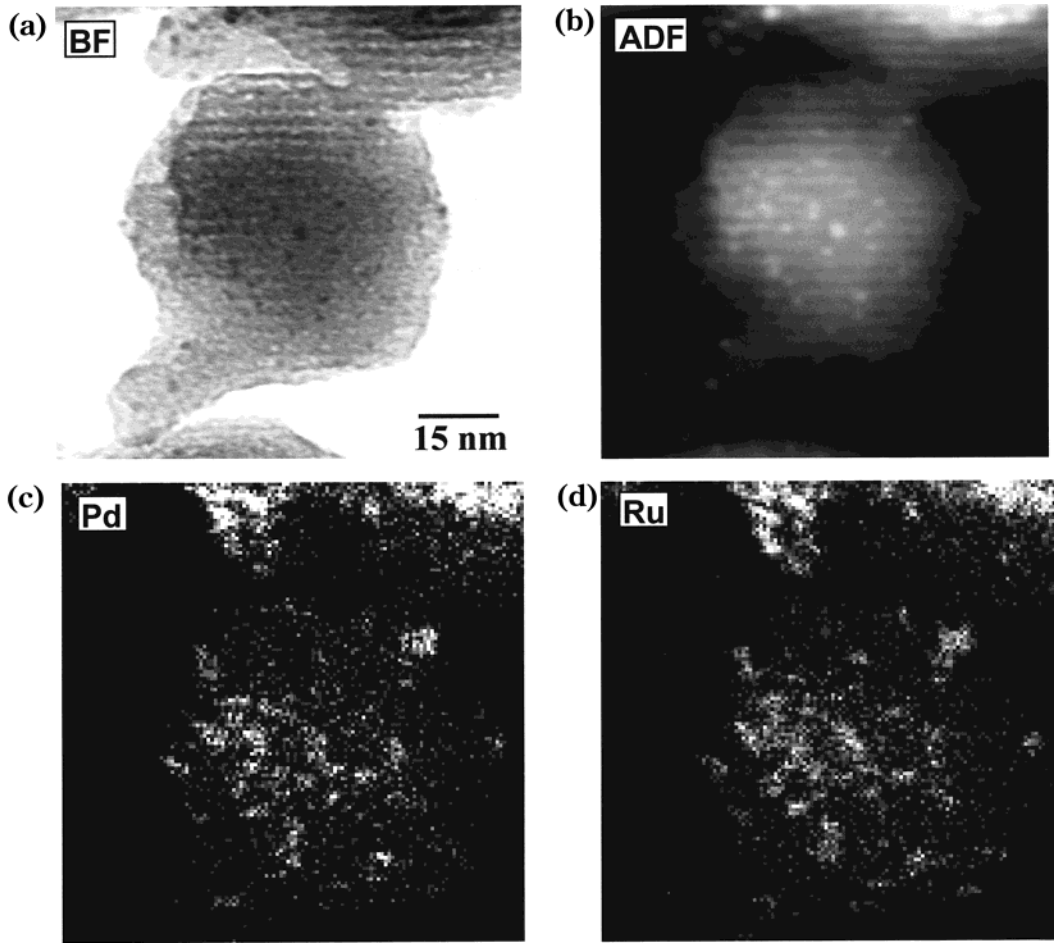

FIGURE 10. (a) Bright-field (BF) and (b) HAADF images of mesoporous silica with Pd_6Ru_6 particles. Electron-stimulated X-ray emission images prove that particles are intact.

their catalytically active state (for various hydrogenations). It is to be noted that the annular dark-field (HAADF) image is greatly superior to the bright-field (BF) image. (The latter, arising as it does from electrons scattered to relatively small angles, is prone to contrast reversals with changes in specimen thickness, whereas the former is not.)

(iv) Mixed-Metal Clusters in Mesoporous Silicas. X-ray-based methods are not well-suited for the structural elucidation of mesoporous materials, chiefly because of the paucity of *hkl* reflections that they yield. Usually, all that may be deduced from the X-ray diffraction patterns of mesoporous silicas, apart from proof of the ordering of the mesopores, is the crystallographic phase and space group to which it belongs. Mesoporous silicas (e.g., MCM-41 and FSM-16) have a cylindrical (ID) system of channels. But there are many other mesoporous silica phases, like the cubic one MCM-48,[37] which have the gyroid surface (see Figure 3).

The structure of the mesoporous silica known as SBA-2 has been greatly clarified by HRTEM[20] and electron crystallography.[44] HRTEM, through micrographs such as those shown in Figure 11,[20] reveals the nature of the complete channel system. We note that, as well as the AB stacking (along [001]) in SBA-2, there are regions of another polytype with ABC stacking (compare EMT and FAU polytypes in faujasitic zeolites depicted in Figure 6

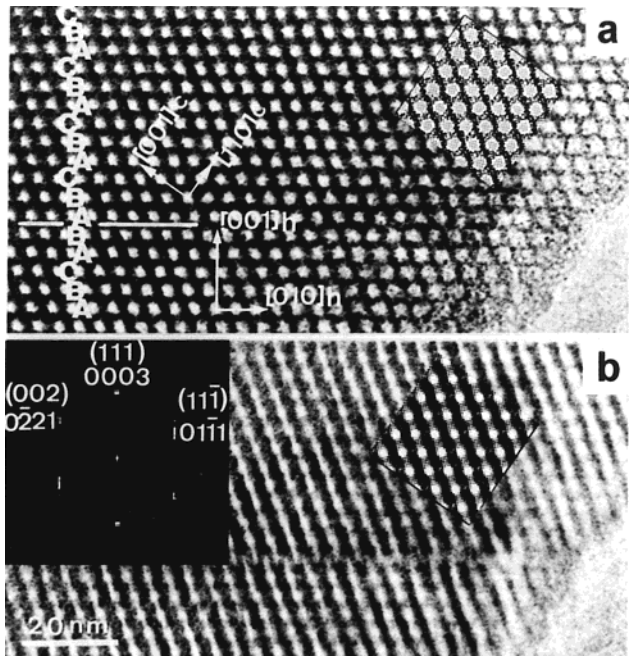

FIGURE 11. HRTEM, computed images, and electron diffraction (in (b)) along two different directions. Cubic (ABC stacking) and hexagonal (AB) polytopic intergrowths occur in a material known as STAC-1.

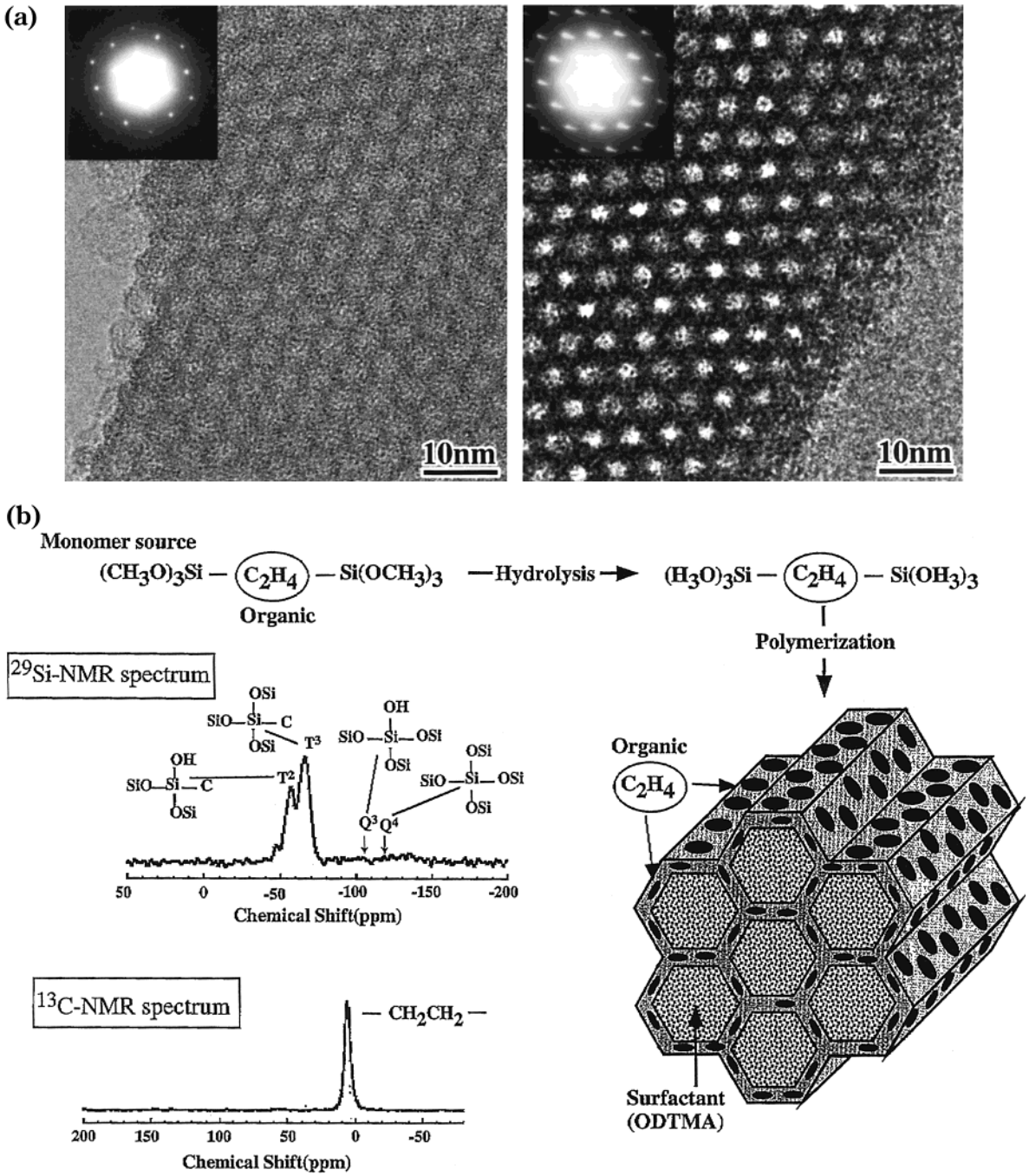

FIGURE 12. (a) HRTEM images and diffraction patterns of novel hybrid structure (see (b)) before removal of templating surfactant. (b) Electron crystallography yields structural principles on which the hybrid with a network of $SiO_{1.5}-CH_2-CH_2-SiO_{1.5}$ is based.

above). This new mesoporous phase is designated STAC-1.[20] HRTEM has also revealed[15] the remarkable tightly packed ordering of anionic ruthenium cluster carbonylates $[Ru_6C(CO)_{16}]^{2-}$ or $[H_2Ru_{16}(CO)_{25}]$ (interspersed with bulky organic cations) along, and perpendicular to, the pores of MCM-41.

(v) The Structure of Mesoporous Solids with Hybrid Organic−Inorganic Networks in the Framework. Materials of this kind have recently been synthesized[50] by condensation of an organosilane compound such as 1,2-bis(trimethoxysilyl)ethane $[(CH_3O)_3Si-CH_2-CH_2-Si(OCH_3)_3]$, BTME, in the presence of alkyltrimethylammonium surfactants, such as octatrimethylammonium (ODTMA) chloride. Adsorption studies, magic-angle-spinning NMR, X-ray diffraction, HRTEM, and electron diffraction leave little doubt that "ethane fragments" are sandwiched by silicons inside the framework of the resulting mesoporous solids. This highly ordered mesoporous structure, schematized in Figure 12, retains its essential structural integrity even after decomposition of the ethane fragments.

6. Future Trends

In addition to being able to cope with the structure determination of beam-sensitive micro- and mesoporous

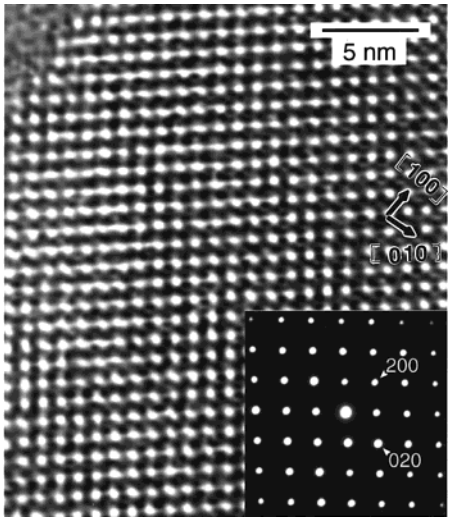

FIGURE 13. HRTEM of a MnAlPO oxidation catalyst exposed to 0.5 bar of H_2. The resolution under these gas "environmental" conditions is adequate to reveal the micropore structure (MnAlPO-18 along [001], with $a = 13.7$ Å, $b = 12.7$ Å, and $c = 18.6$ Å).

materials by the various methods described above, many other developments in electron microscopy now underway are likely to contribute to further structural and physicochemical elucidation. Prominent among these are the following:

(a) in situ environmental high-resolution transmission electron microscopy (EHREM) for direct atomic-scale probing of dynamic gas−solid interactions;[51]

(b) energy-filtered transmission electron microscopy (EFTEM) for the elemental mapping of "frozen" particles;

(c) combined HR(S)TEM and low-voltage scanning electron microscopy (SEM) for surface analysis;[52]

(d) Cathodoluminescence imaging of promoter distribution in working catalysts using photons in SEM, and

(e) photoemission electron microscopy (PEEM) using synchrotron radiation as the primary beam.

(f) Z-contrast tomography, which is a new three-dimensional nanostructural tool based on Rutherford scattering.[53]

One of us (P.L.G.) has shown that high-quality HRTEM images (see Figure 13) may be obtained when the sample itself is in contact with gas at 0.1 bar pressure or more.

Moreover, dynamic in situ studies are possible and thus can reveal structural changes and novel solid-state transformation such as the shear-glide mechanism of Gai[54] discovered in vanadyl pyrophosphate catalysts in the selective oxidation of alkanes. Direct imaging of dynamic liquid polymerization reactions in the production of polyamides shows that nanoscale studies of liquid−solid interactions are now possible.[55] If the advantages of low-voltage SEM—shown by Boyes[52] to be exceptionally well-suited for the determination of the surface composition of the oxides of silicon and aluminum—can be married to the numerous ones possessed by HR(S)TEM, the applicability of the electron optical techniques outlined here will be greatly extended. At present, PEEM is in its infancy, but already spatial resolutions of ca. 25 nm at solid surfaces have been reached.

References

(1) Bursill, L. A.; Lodge, E. A.; Thomas, J. M. Zeolitic structures as revealed by high-resolution electron microscopy. *Nature* **1980**, *286*, 111−113.
(2) Wilson, S. T.; Lok, B. M.; Messina, C. A.; Cannan, T. P.; Flanigen, E. M. Aluminophosphate molecular sieves: a new class of microporous crystalline solids. *J. Am. Chem. Soc.* **1982**, *104*, 1146−1147.
(3) Wright, P. A.; Natarajan, S.; Thomas, J. M.; Bell, R. G.; Gai. P. L.; Jones, R. H.; Chen, J. Solving the structure of a metal-substituted aluminium phosphate by electron microscopy, computer simulation and X-ray powder diffraction. *Angew. Chem., Int. Ed. Engl.* **1992**, *31*, 1472−1475.
(4) Wright, P. A.; Jones, R. H.; Natarajan, S.; Bell, R. G.; Chem, J.; Hursthouse, M. B.; Thomas, J. M. Synthesis and structure of a novel large-pore microporous magnesium-containing aluminophosphates. *J. Chem. Soc., Chem. Commun.* **1993**, 633−635.
(5) Anderson, M. W.; Terasaki, O.; Ohsuna, T.; Philippou, I.; Mackay, S. P.; Rocha, J.; Lidin, S. Structure of titanosilicate ETS-10. *Nature* **1994**, *367*, 347−351.
(6) Thomas, J. M.; Raja, R.; Sankar, G.; Bell, R. G. Molecular-sieve catalysts for the selective oxidation of linear alkanes by molecular oxygen. *Nature* **1999**, *398*, 227−230.
(7) Inagaki, S.; Fukushima, Y.; Kuroda, K. Synthesis of highly ordered mesoporous materials from layered polysilicates. *J Chem. Soc., Chem. Commun.* **1993**, 680−682.
(8) Beck, J. S.; Vartuli, J. C. Recent advances in the synthesis, characterization and applications of mesoporous molecular sieves. *Curr. Opin. Solid State Mater. Sci.* 1996, *I*, 76−87.
(9) Lewis, D. W.; Willcock, D. J.; Catlow, C. R. A.; Thomas, J. M.; Hutchings, G. J. *De Novo* design of structure-directing agents for the synthesis of microporous solids. *Nature* **1996**, *382*, 604−606.
(10) Cheetham, A. K.; Ferey, G.; Loisea, T. Open-framework Inorganic Materials. *Angew. Chem., Int. Ed. Engl.* **1999**, *38*, 3268−3292.
(11) Maschmeyer, T.; Rey, F.; Sankar, G.; Thomas, J. M. Heterogeneous Catalysts obtained by grafting metallocen complexes onto mesoporous silica. *Nature* **1995**, *378*, 159−162.
(12) Thomas, J. M. Design, Synthesis, and *in situ* characterization of new solid catalysts. *Angew. Chem., Int. Ed. Engl.* **1999**, *38*, 3588−3628.
(13) Thomas, J. M. New microcrystalline catalysts. *Philos. Trans. R. Soc. London*, *Ser. A* **1990**, *333*, 173.
(14) (a) Thomas, J. M. The high-resolution structural characterization and the rational design of inorganic solid catalysts. *Faraday Discuss.* **1996**, *105*, 1−31. (b) Thomas, J. M.; Maschmeyer, T.; Johnson, B. F. G.; Shephard, D. S. Constrained chiral catalysts. *J. Mol. Catal.* **1999**, *141*, 139−144.
(15) Zhou, W.; Thomas, J. M.; Shephard, D. S.; Johnson, B. F. G.; Ozkaya, D.; Maschmeyer, T.; Bell, R. G.; Ge Oingfe, Ordering of ruthenium cluster carbonyls in mesoporous silica. *Science* **1998**, *280*, 705−708.
(16) Sankar, G.; Jones, R. H.; Thomas, J. M.; Catlow, C. R. A.; Lewis, D. N.; Clegg, W.; Coles, S. J.; Teat, S. J. Structure of templated microcrystaline DAF-5 determined by synchrotron diffraction. *J. Chem. Soc.*, *Chem. Commun.* **1998**, 117−118.
(17) Harris, K. D. M.; Tremayne, M.; Karuki, B. M. Contemporary advances in use of powder x-ray diffraction for structure determination. *Angew. Chem., Int. Ed.* **2001**, *40* (in press).
(18) (a) Thomas, J. M.; Millward, G. R. Direct real-space determination of intergrowths in ZSM-5/2SM-11 catalysts. *J. Chem. Soc., Chem. Commun.* **1982**, 1380−1382.
(19) Terasaki, O.; Ohsuna, T.; Alfredsson, V.; Bovin, J.-O.; Watanabe, D.; Anderson, M. W. Observations of spatially correlated intergrowth of Faujasitic polytypes and the pure end members by high-resolution microscopy. *Chem. Mater.* **1993**, *5*, 452−458.
(20) Zhou, W.; Hunter, H. M. A.; Wright, P. A.; Ge, Q.; Thomas, J. M. Imaging the pore structure and polytypic intergrowths in mesoporous silica. *J. Phys. Chem.* 1998, *102*, 6933−6936.
(21) Thomas, J. M. High-resolution electron microscopy and electron energy loss spectroscopy. In *Inorganic Chemisty: towards the 21st Century*; Chisholm, M. H., Ed.; ACS Series 211; American Chemical Society: Washington, DC, **1983**; pp 445−472.
(22) Ozkaya, D.; Zhou, W.; Thomas, J. M.; Midgley, P. A.; Keast, V. J.; Hermans, S. High-resolution imaging on nanoparticle bimetallic catalysts supported on mesoporous silica. *Catal. Lett.* **1999**, *60*, 113−120.

(23) Terasaki, O.; Yamazaki, K.; Thomas, J. M.; Ohsuna, T.; Watanabe, D.; Sanders, J. V.; Barry, J. C. Isolating individual chains of selenium by incorporation into the channels of a zeolite. *Nature* **1987**, *330*, 58−60.
(24) Allpress, J. G.; Sanders, J. V. The Direct observation of the structure of real crystals by lattice imaging. *J. Appl. Crystallogr.* **1973**, *6*, 165−190.
(25) Thomas, J. M.; Jefferson, D. A. Where is high-resolution electron microscopy taking us? *Endeavour* **1979**, *2*, 127−130.
(26) Thomas, J. M.; Jefferson, D. A.; Smith, D. J.; Crawford, E. S. The elucidation of the ultrastructure of silicate mineral by high-resolution electron microscopy and X-ray emission microanalysis. *Chem. Scr.* **1978/79**, *14*, 167−179.
(27) Mallinson, L. G.; Thomas, J. M.; Jefferson, D. A.; Hutchison, J. L. The internal structure of nephrite: multiple-chain silicates within an amphibole host. *Philos. Trans. R. Soc. London, Ser. A* **1980**, *295,* 537−552.
(28) Crawford, E. S.; Jefferson, D. A.; Thomas, J. M.; Bishop, A. C. Structure−composition relationships in the serpentine minerals by combined X-ray emission and high-resolution microscopy. *J. Chem. Soc., Chem. Commun.* **1978**, 986−987.
(29) Jefferson, D. A.; Thomas, J. M. Electron microscopic and X-ray studies of non-random disorder in chloritoid, an unusual layered silicate. *Proc. R. Soc. London, Ser. A* **1978**, *361*, 399−411.
(30) Evans, E. L.; Thomas, J. M. An electron microscopic study of the ultrastructure of some graphite intercalates. *J. Solid State Chem.* **1975**, *14*, 99−121.
(31) Thomas, J. M.; Audier, M.; Millward, G. R.; Ramdas, S.; Bursill, L. A. New methods for the structural characterization of shape-selective zeolites. *Faraday Discuss.* **1981**, *72*, 345−352.
(32) Ohnishi, N,; Hiraga, K. Slow-scan CCD camera analyis of electron diffaction and high-resolution micrographs of zeolite TPA/ZSM-5. *J. Electron Microsc.* **1996**, *45*, 85−92.
(33) Nicolopoulos, S.; Gonzalez-Calbet, J. M.; Vallet-Regi, M.; Corma, A.; Conell, C.; Guil, J. M.; Perez-Paniente, J. Direct phasing in electron crystallography: *ab initio* determination of a new zeolite structure MCM-22. *J. Am. Chem. Soc.* **1995**, *117*, 8947−8956.
(34) Klug, A. Presented at the Chemistry Nobel Prize Lecture, Nobel Foundation, Stockholm, 1982; pp 93−125.
(35) (a) Cowley, J. M. *Diffraction Physics;* North-Holland: Amsterdam, 1984. (b) Terasaki, O.; Thomas, J. M.; Watanabe, D.; Millward, G. R. The role of HREM in the identification and characterization of new crystalline microporous materials: 'reading off' the structure and symmetry elements of pentasil molecular sieves. *Chem. Mater.* **1989**, *1*, 158−165.
(36) Hovmoeller, S. CRISP—Crystallographic image—processing with a personal computer. *Ultramicroscopy* **1992**, *41*, 121−135.
(37) Carlsson, A.; Kaneda, M.; Sakamoto, Y.; Terasaki, O.; Ryoo, R.; Joo, S. H. The structure of MCM-48 determined by electron crystallography. *J. Electron Microsc.* **1999**, *48*, 795.
(38) Vaughan, D. E. W.; Treacy, M. M. J.; Newsam, J. M. Recent advances in techniques for characterizing zeolite structures. In *Guidelines for Mastering the Properties of Molecular Sieves*; Barthomeuf, D., Ed.; Pleasure Press: New York, 1999; pp 99−120.
(39) (a) Ozkaya, D.; Thomas, J. M.; Shephard, D. S.; Maschmeyer, T.; Johnson, B. F. G.; Sankar, G.; STEM analyses of bimetallic catalysts in mesoporous MCM-41. *Proc. Inst. Phys. Electron Microsc. Anal. Group Conf.* **1997**, 403−406. (b) Thomas, J. M.; Williams, B. G.; Sparrow, T.; Uppal, M. K. Chemical analysis and studies of electronic structure of solids by EELS with an electron microscope. *Philos. Trans. R. Soc. London, Ser. A* **1984**, *311,* 271−285.
(40) Leonowicz, M. E.; Vaughan, D. E. W. Proposed synthetic zeolite ECR-1 structure gives a new zeolite framework topology. *Nature* **1987**, *329*, 819−821.
(41) Thomas, J. M.; Millward, G. R.; White, D.; Ramas, S. Direct evidence to support the proposal that ZSM-23 is a recurrently twinned variant of zeolite theta-1. *J. Chem. Soc., Chem. Commun.* **1988**, 434−436.
(42) Barri, S. A. I.; Smith, G. W.; White, D.; Young, D. New zeolite Theta-1. *Nature* **1984**, *312*, 533−535.
(43) Terasaki, O.; Thomas, J. M.; Ramdas, S. A new type of stacking fault in zeolites: presence of a coincidence boundary ($\sqrt{13})\sqrt{13}$ R32.2° superstructure) perpendicular to the tunnel direction in zeolite-L *J. Chem. Soc., Chem. Commun.* **1984**, 216−217.
(44) (a) Wright, P. A.; Natarajan, S.; Thomas, J. M.; Gai-Boyes, P. L.; Jones, R. H.; Chen, J. Solving the structure of a metal-substituted aluminium phosphate catalyst by electron microscopy, computer simulation and X-ray powder diffraction. *Angew. Chem., Int. Ed. Engl.* **1992**, *31*, 1472−1475. (b) Wagner, P.; Terasaki, O.; Ritsch, S.; Nery, J. G.; Zones, S. I.; Davis, M. E. Electron diffraction structure solution of a nanocrystalline zeolite at atomic resolution. *J. Phys. Chem. B* **1999**, *103*, 8245−8250.
(45) Gai-Boyes, P. L.; Thomas, J. M. T.; Wright, P. A.; Jones, R. H.; Natarajan, S.; Chen, J.; Xu, R. Real-space imaging of molecular sieves composed of aluminophospates and their metal-substituted analogues. *J. Phys. Chem.* **1992**, *96*, 8206−8209.
(46) Baerlocher, C.; Heppe, A.; Meier, W. *A Distance-least-squares manual. DLS-76;* Institute of Crystallography and Petrology, ETH: Zurich, 1977.
(47) Catlow, C. R. A.; Thomas, J. M.; Wright, P. A.; Bell, R. G.; Freeman, C. M. Simulating and predicting crystal structures. *Proc. R. Soc. London, Ser. A* **1993**, *442*, 85−96.
(48) Bovin, J. O.; Alfredsson, V.; Karlsson, G.; Carlsson, A.; Blum, A.; Terasaki, O.; TEM-tomography of FAU-zeolite crystalls containing Pt-clusters. *Ultramicroscopy* **1996**, *62,* 277.
(49) Raja, R.; Hermans, S.; Bromley, S.; Shephard, D. S.; Maschmeyer, T.; Thomas, J. M.; Johnson, B. F. G. Preparation and characterization of a highly active bimetallic (Pd−Ru) nanoparticle heterogeneous catalyst. *Chem. Commun.* **1999**, 1571−1572.
(50) Inagaki, S.; Guan, S.; Fukushima, Y.; Oksuna, T.; Terasaki, O.; Ordered Mesoporous Materials. *Stud. Surf. Sci. Catal.* **2000**, *129*, 155−162.
(51) Gai, P. L. Environmental high-resolution electron microscopy of gas−solid reactions. *Top. Catal.* **1999**, *8*, 97−113.
(52) Boyes, E. D. On low voltage scanning electron microscopy and chemical microanalysis. *Microsc. Microanal.* **2000**, *6*, 307−316.
(53) Midgley, P. A.; Weyland, M.; Thomas, J. M.; Johnson, B. F. G. Z-contrast tomography: A technique in 3-Dimensional Nano-structural Analysis based on Rutherford scattering. *Chem. Commun.* **2001** (in press).
(54) Gai, P. L. A new structural transformation mechanism in catalytic oxides. *Acta Crystallogr.* **1997**, *1353*, 346−352.
(55) Gai, P. L.; Kourtakis K.; Ziemecki, S. *Microsc. Microanal.* **2000**, *6*, 335−342.

AR970352J